FAN-INTAKE INTERACTION UNDER HIGH INCIDENCE

Teng Cao,
Nagabhushana Rao Vadlamani,
Paul G Tucker

Department of Engineering,
University of Cambridge

Angus R. Smith,
Michal Slaby,
Christopher T. J. Sheaf

Civil Installation Aerodynamics,
Rolls-Royce plc,
Derby

ABSTRACT

In this paper, we present an extensive numerical study on the interaction between the downstream fan and the flow separating over an intake under high incidence. The objectives of this investigation are twofold: (a) to gain qualitative insight into the mechanism of fan-intake interaction and (b) to quantitatively examine the effect of the proximity of the fan on the inlet distortion. The fan proximity is altered using the key design parameter, L/D, where D is the diameter of the intake and L is the distance of the fan from the intake lip.

Both steady and unsteady Reynolds Averaged Numerical Simulations (RANS) were carried out. For the steady calculations, a low order fan model has been used while a full 3D geometry has been used for the unsteady RANS. The numerical methodology is also thoroughly validated against the measurements for the intake-only and fan-only configurations on a high bypass ratio turbofan intake and fan respectively. To systematically study the effect of fan on the intake separation and explore the design criteria, a simplified intake-fan configuration has been considered. In this fan-intake model, the proximity of the fan to the intake separation (L/D) can be conveniently altered without affecting other parameters.

The key results indicate that, depending on L/D, the fan has either suppressed the level of the post-separation distortion or increased the separation-free operating range. At the lowest L/D (~ 0.17), around a 5° increase in the separation-free angle of incidence was achieved. This delay in the separation-free angle of incidence decreased with increasing L/D. At the largest L/D (~ 0.44), the fan was effective in suppressing the post-separation distortion rather than entirely eliminating the separation. Isentropic Mach number distribution over the intake lip for different L/D's revealed that the fan accelerates the flow near the casing upstream of the fan face, thereby decreasing the distortion level in the immediate vicinity. However, this acceleration effect decayed rapidly with increasing upstream distance from the fan-face.

INTRODUCTION

The next-generation aircraft engines operate at a high bypass and low fan pressure ratios. The intakes of such aero engines have a larger diameter and thus require a shorter length to compensate for the increase in the drag. However, when compared to the conventional intakes, shorter intakes suffer from reduced diffusion capability which can cause the flow to separate more easily on the nacelle, specifically under off-design conditions. There is also a potential for an increased aerodynamic interaction between the intake and downstream fan. The overall performance is sensitive to this interaction of the separated flow with the fan.
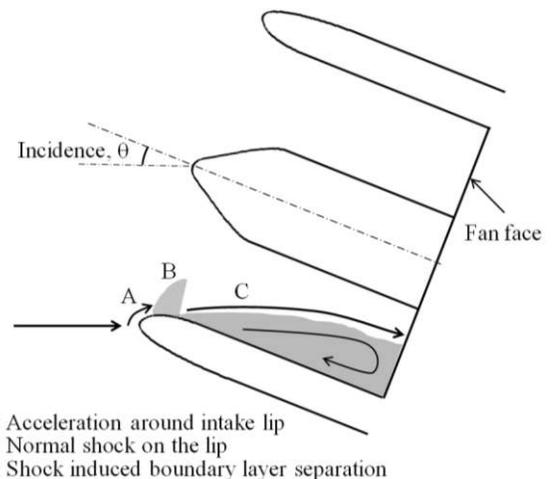
Fig. 1: Schematic showing the flow physics around an intake operating under a typical off-design high-incidence condition

The flow past an intake lip is highly complex, specifically under off-design conditions. It has several zones with contrasting flow physics as illustrated in Fig. 1. These include zones of (a) accelerating flow around the intake lip (b) shock induced boundary layer separation and (c) transition to turbulence. Under the off-design operating conditions of higher angles of incidence or due to severe crosswinds, the flow separates on the lip. The separated flow is inherently unstable and undergoes transition to turbulence. The size of the separation determines the distortion at the fan face which will influence the performance of the fan and its compatibility.

Previous work:
An improved understanding of the intake aerodynamics and its interaction with the fan is hence crucial in developing the modern aircraft engines. Extensive studies were carried out in the literature by various researchers to address this issue. These

studies can be broadly classified into the following categories, which explored the effect of the: (a) Off-design conditions like high-incidence and crosswinds on the intake-only configuration [1] and the hysteresis phenomena associated with flow separation and reattachment [2]; (b) Inlet distortion on the stability of the fan [3] ; (c) Fan-intake interaction on the incidence tolerance [4], [5] and the subsequent optimization of the intake shape [6].

Since the current paper is primarily concerned about the fan-intake interaction under high incidence, the associated experimental and numerical studies have been reviewed below:

Experimental investigations: Hodder [7] conducted tests on the inlet performance at high angles-of-attack with the inlet coupled and decoupled to the downstream engine. The results suggested that the engine has an attenuation effect of the inlet separation thereby allowing the inlet to operate at lower levels of distortion. Larkin and Schweiger [4] conducted a scaled inlet test program to investigate the impact of the fan on inlet separation when operating at large angles of attack. Contrary to Hodder's [7] findings, it was observed that the presence of fan improved the incidence tolerance by about 3-4°. This delay of the onset of flow separation observed in a powered inlet operation was also duplicated by placing struts (which create blockage) at the fan face. Boldman et al. [5] presented a comprehensive experimental work investigating the effect of rotating propeller on the intake separation angle of attack. It was demonstrated the propeller has increased the separation-free angle of attack by 2.7-4°, when compared to a clean inlet without fan, depending on the operating mass flow. A similar amount of delay in the separation angle of attack was achieved by an aspirated flow with a blockage device.

Numerical investigations using CFD (Computational Fluid Dynamics): Following Hodder's work [7] , Kennedy et al. [8] numerically studied the intake performance under high incidence. In these simulations, the full 3D fan geometry was modeled. Consistent with Hodder's observations, two main effects of fan: attenuation of the inlet distortion and the redistribution of the upstream flow, were well captured by the numerical method. Hsiao et al. [9] investigated powered-nacelle aerodynamics using an actuator duct model to represent the fan. A considerable suppression effect by the fan on nacelle separation has been captured. It was also claimed that for the powered-nacelle, the presence of the fan rotor increased the separation-free angle of attack over the nacelle by 3°, which is consistent with experimental observations. Iek et al. [10] carried out numerical investigations on the intake-fan interaction under different angles of attack. A simple screen boundary condition (BC), which creates blockage to the flow, was incorporated to represent the effect of fan. Interestingly, there wasn't any sign of delay in the angle at which the flow separated. However, once the flow separates, evidence suggests that the blockage induced by the screen BC was capable of suppressing the flow distortion. Carnevale et al. [11] carried out a computational study into flow separation in a subsonic civil aircraft intake and its interaction with downstream fan. Both steady and unsteady RANS models were respectively used to simulate the isolated intake and powered intake configurations. It was shown that the fan stage is beneficial in increasing the tolerance to flow incidence and suppressing the flow distortion. Peter et al. [6] presented an integrated fan-nacelle design framework based on CFD with the fan incorporated using a bulk body force model (BFM). A parametric study of the influence of intake-fan interaction on overall engine performance was conducted. It was identified that the interaction of the fan rotor with the high streamwise Mach number on the intake lip was the bottleneck for design of short inlets. It was therefore concluded that a trade-off between the length of inlets and fan face Mach number has to be made in order to achieve an optimum overall engine performance.

Metrics:

Determining the inlet distortion level and the onset of inlet lip separation is an important aspect of the intake studies. The total pressure distortion at the fan face is typically measured using the distortion coefficient DC60, defined as:

$$DC60 = (P_{0,60} - P_0)/(P_0 - P)$$

where P_0 and P are the area weighted average total and static pressures at the fan face and $P_{0,60}$ is the area averaged total pressure for the 60° segment with the lowest mean total pressure. It provides a measure of the difference between average total pressure level at the intake inlet and the average total pressure level of the worst 60° at the aerodynamic interface plane. Separation is usually determined if a steep increase in distortion coefficient, DC60, is observed beyond a critical angle of attack.

Scope of this paper:

It is apparent from the review that the fan is capable of reducing the level of inlet distortion once the flow has separated. However, the conditions under which the fan could improve the incidence tolerance are not evident. The intake-fan interaction mechanism responsible for the suppression of the flow separation is also not clear. This leads to the key objectives of the current paper, which are twofold:

(a) To gain qualitative insight into the mechanism of fan-intake interaction and

(b) To quantitatively examine the effect of the proximity of the fan on the inlet distortion. The fan proximity is altered using the key design parameter, *L/D*, where *D* is the diameter of the intake and *L* is the distance of the fan from the intake lip.

An extensive numerical study on the interaction between a downstream fan and the flow separating over an intake at high incidence will be addressed. The simulations were performed using RANS coupled with a low order model to represent fan. In the first part of the paper, the numerical framework has been validated against both the experiments and a high fidelity unsteady RANS on a real engine and fan configurations. In the

second part, a simplified intake-fan configuration has been considered to systematically study the influence of the axial location of the fan (by varying *L/D*) on the inlet distortion. In this fan-intake model, the ratio of the intake length to diameter (*L/D*) can be conveniently altered without affecting other parameters.

NUMERICAL METHODOLOGY

Configurations: Fig. 2(a,b,c) show the three different configurations considered in this study. These include:
A: High bypass intake-only and intake-BFM configurations for the steady RANS simulations.
B: High bypass intake with fully represented fan geometry for the unsteady RANS simulations.
C: An axis-symmetric intake for the RANS simulations on a 'model intake'.
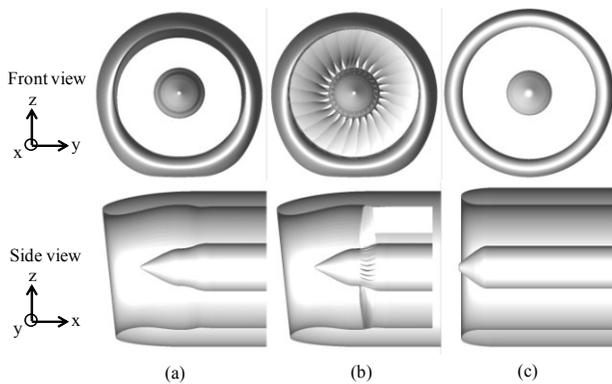
Fig. 2: Configuration considered for: a) RANS on Intake-only and Intake-BFM b) Unsteady RANS with full fan representation c) RANS on Model intake

Meshing: As described in the introduction, the critical flow features over an intake operating under high incidence include: a normal shock over the intake lip, separated shear layer after the normal shock and the zone of interaction between the separated flow and the fan (which is either fully resolved or represented using a BFM). Sufficient care has to be taken to satisfactorily capture these flow features using finer meshes, yet considering economical measures to reduce the computational cost. While a fully structured mesh results in a substantial increase in the mesh density in the free-stream, an unstructured mesh leads to deteriorated performance in the boundary layers. Thus, a hybrid meshing strategy was employed to mesh the geometries. For all the configurations, the near-wall (intake and spinner) and the body-force regions were meshed using the structured hexahedral elements since these elements provide an improved boundary layer resolution. The free-stream domain was meshed using the unstructured tetrahedral elements. Fig. 3(a) shows the hybrid mesh and the corresponding insets show the magnified view of the mesh distribution around the top and bottom lips of the intake.

In all the simulations, standard Spalart-Allmaras (SA) turbulence model with wall functions was used to account for the eddy viscosity. The wall functions allowed for a coarser mesh to be employed in the near-wall region, corresponding to y^+ values of 20-30 whilst still maintaining satisfactory boundary layer treatment. Meshes with much lower values of y^+ have also been used; however, it was observed that the number of circumferential points required maintaining appropriate cell aspect ratio increases enormously, without any noticeable change in the solution. Low Mach number preconditioning has also been used to obtain a better prediction of the low Mach separated flow regions. It must be noted that the use of different turbulence models will quantitatively influence the solution to some extent. However, given that the interaction between the fan and the separation over the intake is largely due to the inviscid dynamics, the conclusions drawn from this study would remain the same by using a different turbulence models.

Computational cost: Around 14×10^6, 75×10^6 and 8×10^6 cells were used to mesh the configurations A, B and C respectively. Most cells (~ 90%) were clustered around the intake and the body-force (or fan) while the rest of them (~ 10%) were used in the free-stream. For the full-annulus unsteady RANS calculation (configuration B), each blade passage was spatially resolved with 2.5×10^6 cells and temporally resolved with 80 physical time steps. Simulations were carried out for 15 full revolutions before collecting the averaged solution for the final revolution. The total run time of the unsteady RANS calculation is around 300 hours (12.5 days) using 480 processors on the UK national supercomputing service, ARCHER.

CFD setup and methodology to estimate separation angle: As illustrated in Fig. 3(b), a no-slip condition was imposed on the intake and spinner walls. Free-stream values were specified in the far-field and a mass flow boundary condition was specified at the exit. The free-stream values correspond to the atmospheric conditions of density, pressure and temperature at an altitude ranging between 15000-17000ft. The ratio of turbulent to laminar viscosity ratio was set to 10 in the free-stream. An additional constraint of radial equilibrium has been imposed at the exit for the simulations which considered the effect of fan. It was ensured that the normalized mass flow $(\dot{m}\sqrt{T_0}/P_0)$ into the engine is within 0.1% of the desired value for all the calculations reported. The exit boundary condition applied is a static pressure condition with radial equilibrium. The solver iteratively adjusts the exit static pressure to achieve the desired mass flow.
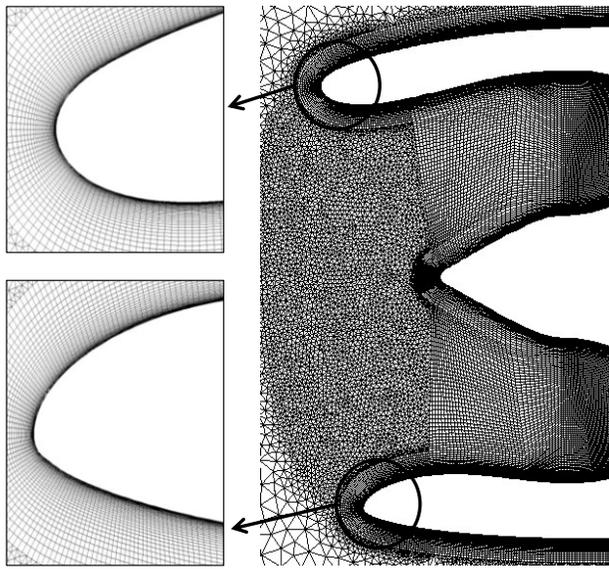
(a)
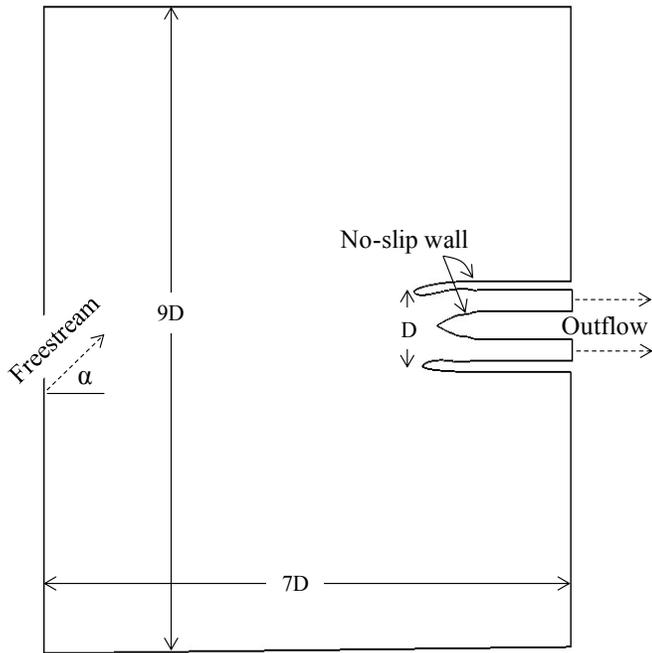
(b)

Fig. 3: (a) Hybrid meshing strategy: Structured hexahedral elements around the intake lips, spinner and body force regions and unstructured tetrahedral meshing in the free-stream (b) Computational domain with the imposed boundary conditions

To identify the angle, α_{sep}, at which the flow separates over the intake, an initial simulation was obtained at an incidence angle which was approximately 5° away from the known/estimated separation incidence, i.e. at (α_{sep} - 5)°. A series of simulations were then carried out with an increasing incidence of 1° using the solution from the previous run to

initialize the current simulation. The separation angle is identified based on a critical DC60 value. Subsequently, smaller increments of typically 0.25° were taken to accurately identify the separation incidence, α_{sep}.

Solver: All the simulations reported in this paper were carried out using the Rolls-Royce's in-house solver: HYDRA [12]. It is a density, edge-based finite-volume unstructured solver which is second-order accurate in both space and time. It has been largely optimized for parallel computation on the distributed memory Machines. The solver can handle multi-fidelity methods including Reynolds-averaged Navier-Stokes RANS/ unsteady RANS/ Large Eddy Simulations (LES). It has also been validated over a range of complex flows [13]. For the steady simulations, the effect of the fan was represented using the low order model function in HYDRA [14].

VALIDATION

Experimental setup used to validate CFD: Before considering the effect of fan, it is crucial to verify that the computational setup described in the previous section is accurate enough. It should be capable of providing reasonable estimates of the separation angle and the distortion levels. The data used to validate the CFD setup stems from the experiments of ONERA. Measurements were taken over a civil aircraft intake model in a rectangular wind tunnel. The wind tunnel section is 4.5 m wide, 3.5 m high and 11 m long and was able to provide a constant Mach number flow up to 0.36. Around 15 static pressure tapings were instrumented axially over the surface of the intake. Each pressure tapping was scanned and recorded 6 times over a 0.17 second period by the pressure measurement system. An averaged value for each scan was estimated using these values. The accuracies of the pressure and Mach number measurements were within +/- 0.05% and <0.35% dynamic head respectively. The angle of intake was varied between 0 to 35º using the actuators that drive the rotation of the intake. The potentiometers placed over these actuators were used to estimate the angle of the intake within an accuracy range of +/- 0.2º.

Separation estimates of the intake-only configuration: For the intake-only configuration, Fig. 4(a) shows the axial variation of the isentropic Mach number over the intake lip pre and post separation. The corresponding experimental data is also overlaid for comparison. The steady RANS predictions agree favorably with the measurements in terms of capturing the rapid acceleration over the intake lip followed by the normal shock. Once the flow separates, the shock location moves further forward over the intake lip. This phenomenon has also been well predicted in the simulations.
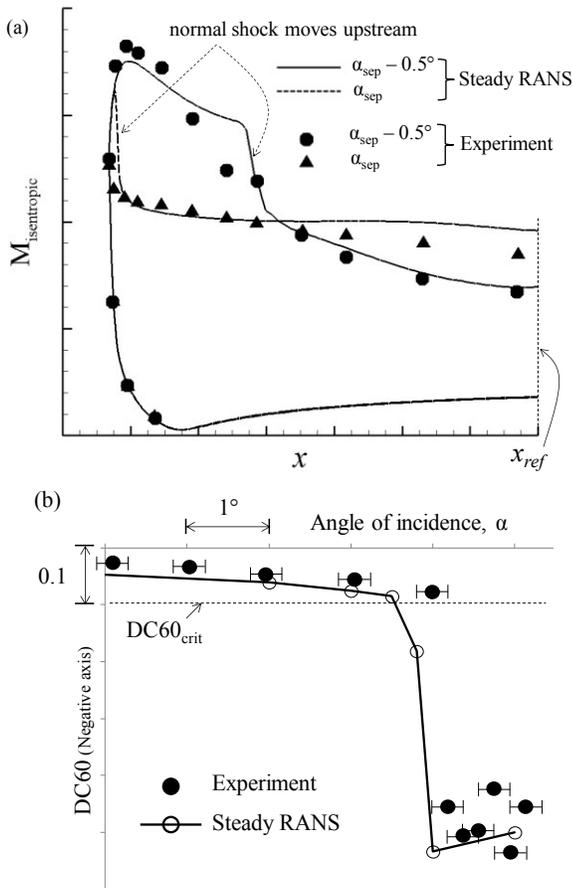
Fig. 4: Variation of a) isentropic Mach number profiles over the intake lip pre and post separation and b) distortion coefficient with increasing incidence for the intake-only case (Error bars correspond to the potentiometer accuracy within +/- 0.2°)

The shock appears to be less intense in the measurements and is not as distinct as that observed in the CFD. This could be attributed to the fact that the pressure tapings in the measurements were distantly spaced thereby reducing the resolution of the shock region. Also, for the post-separated case, a noticeable deviation in Mach number can be observed after the shock. This could be due to the inability of the standalone SA model [15] to handle the complex physics of acceleration, relaminarization, separation and transition to turbulence [1].

Fig. 4(b) compares the predicted values of DC60 against the measurements with increasing incidence. The distortion coefficient is evaluated at an axial location x_{ref} (which corresponds to the fan-face location in the case of simulations with fan). A steep decrease in the DC60 below DC60$_{crit}$ indicates the shock-induced separation. When compared to the measurements, the separation estimates lie within a tolerance of ±0.25° which further validates the current computational methodology.
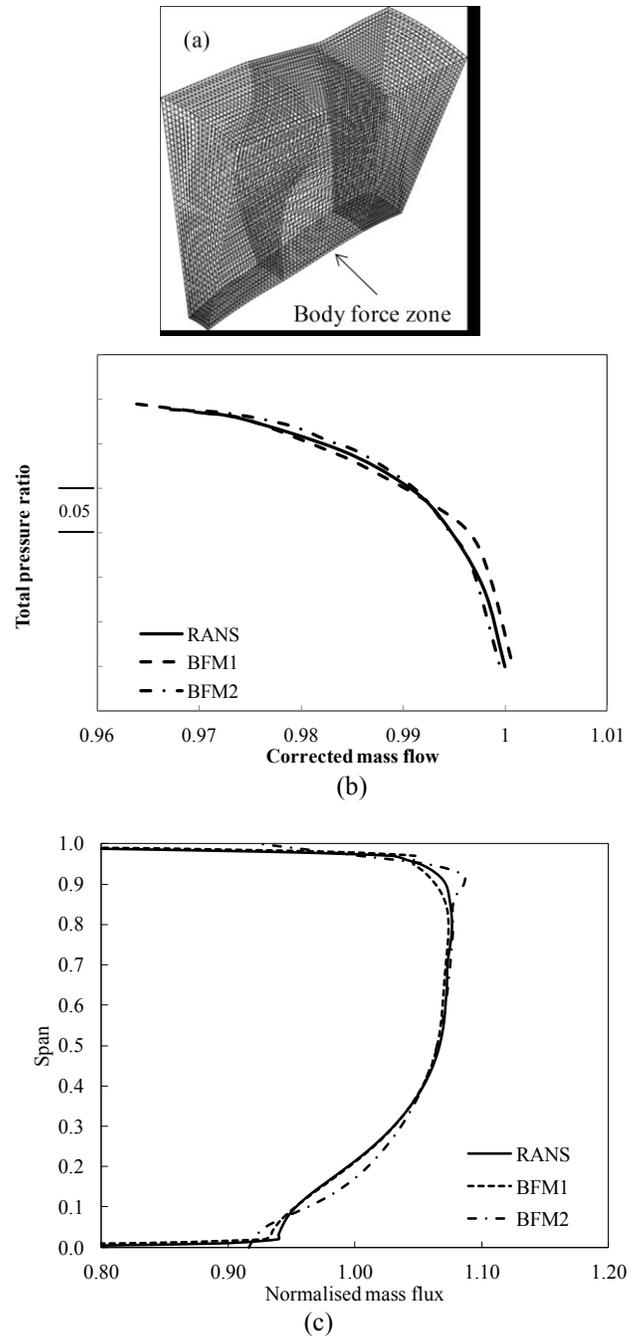
Fig. 5: a) Sector mesh used for the body force simulations; Comparison of b) fan characteristic and c) radial distribution of mass flux predicted by BFM against the RANS with full fan representation.

Performance of body force model: The fan characteristic was calculated using the BFM on a sector mesh shown in Fig. 5(a). The fan characteristic (pressure ratio *vs.* mass flow) was estimated at a design speed of 95.4% which corresponds to the flight climb condition. Two different body force models have been considered. BFM1 is the low order model function in HYDRA [14] and BFM2 is the IBMSG model from Cao et al.

[16]. Fig. 5 (b,c) compares the predictions of both the body force models against the 3D RANS. It is evident that the models are able to correctly predict the pressure rise across the fan including the chocking phenomena. Fig. 5(c) also ensures that the radial distribution of the normalized mass flux is well predicted by the both the models. Although BFM2 is based on a more general theoretical framework, both the models yield a similar level of fidelity. However, all the findings reported in this paper are evaluated using BFM1 since a more complete set of results were available with BFM1 at the time of writing. It is worth pointing out that the incoming small scale turbulence could influence the fan performance. However, this effect would be much smaller when compared to the effect of the large scale distortion which the current framework is capable of capturing reliably.
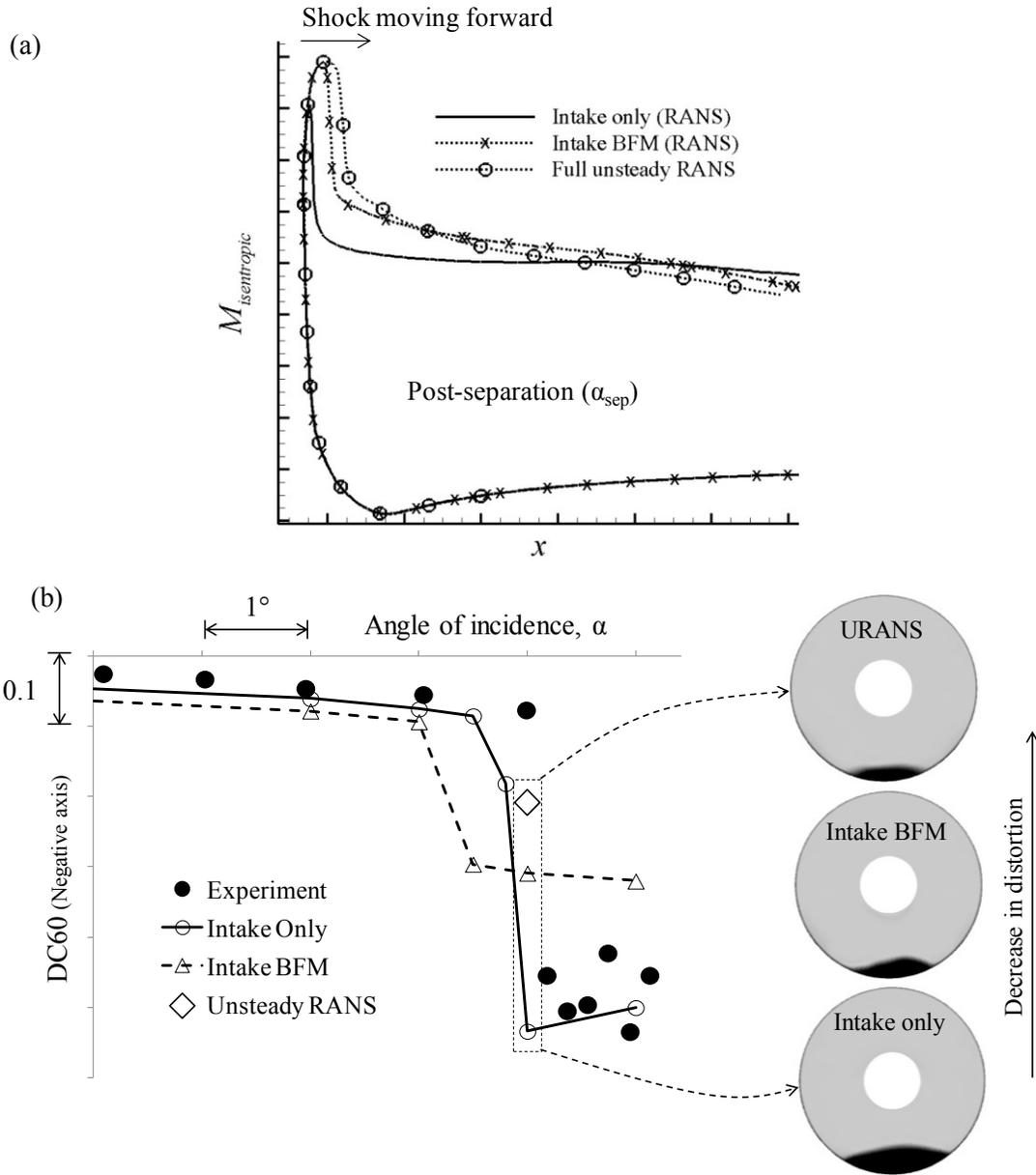

Fig. 6: (a) Axial variation of isentropic Mach number post separation and (b) Variation of distortion coefficient with increasing incidence for configurations A and B (Inset plots show the contours of stagnation pressure at the fan-face

EFFECT OF FAN

Having validated the computational framework, the effect of fan on the flow separating over the intake will be considered in this section. Fig. 6(a) compares the axial variation of the isentropic Mach number over the intake lip with and without fan. Notice that the location of the shock has moved downstream due to the body force. Its impact on the distortion levels at the fan-face, x_{ref}, can be observed from Fig. 6(b). It is evident that there is a decrease in the level of post-separation distortion by almost 25% in the presence of fan. This observation is further reinforced by comparing the contours of stagnation pressure at the fan face. The loss of stagnation pressure at the fan-face is much smaller in the intake-fan case due to a smaller separation. This result is consistent with the experimental observations [7] and the numerical simulations [8, 9]. For configurations A and B, it is reiterated that the fan has only decreased the level of distortion at the fan-face rather than improving the incidence tolerance. It is attributed to a larger L/D of this intake (~ 0.5). This fact will become clearer in the subsequent section on a model intake study where the effect of L/D on the incidence tolerance has been systematically assessed.

It is also essential to verify if the low order body force model predicted a reasonable estimate of the reduction in DC60. Thus, a full annulus unsteady RANS simulation, on configuration B, has been carried out at the separation angle α_{sep}. Fig. 6(a,b) compare the corresponding results from unsteady RANS against the steady intake-fan simulation. The following conclusions were drawn from these plots: a) It can be confirmed that there is a reduction in the post-separation distortion in the presence of fan b) Results predicted by BFM (axial variation of Mach number and contours of stagnation pressure at fan-face) qualitatively agree with those predicted by unsteady RANS c) However, the BFM predicted a larger level of distortion in comparison to unsteady RANS. This is indeed a positive sign for the intake designers, as the steady BFM provides reasonably accurate results (along with a factor of safety on distortion estimates) at a much lower computational cost than unsteady RANS.

MODEL INTAKE STUDY

Design and setup of model intake: To systematically study the effect of the fan on the intake separation and explore the design criteria, a simplified intake-fan configuration has been considered. As mentioned in the earlier sections, the simulations were performed using a steady RANS model with a low order body force model to represent the fan. The design of the simplified model illustrated in Fig. 7 stems from a typical civil style intake and fan operating near choking condition. A constant area duct has been used downstream of the nose-cone of the spinner. The axial position of the fan (and the ratio of the intake length to diameter (L/D)) could thus be conveniently altered over a wide range of *L/D's*.

Firstly, it has been ensured that the model intake-fan configuration is representative of a real engine intake in terms of the separation mechanism. Fig. 8 shows the contours of the isentropic Mach number at two different angles of incidence. Consistent with the case of a real intake, the flow over the intake experiences a shock induced separation once the incidence reaches a critical value.

X_{fixed} $X_{fan\text{-}face}$

Fan Position 1   Fan Position 2
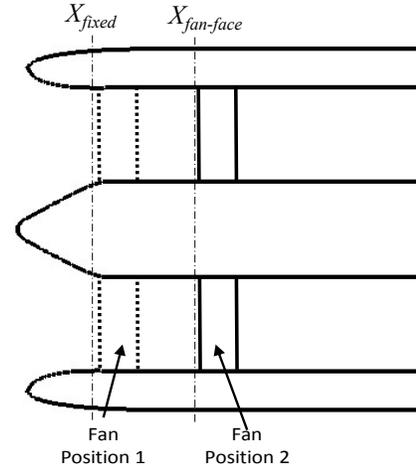
Fig. 7: Sketch of model intake-fan configuration

The effect of the fan at four different axial locations has been considered, corresponding to the *L/D* values of 0.17, 0.20, 0.24 and 0.44. With a fan chord of about 7% of the intake diameter, the difference between the *L/D's* correspond to axially shifting the fan through half, full, and four times of fan chords respectively. DC60 has been evaluated at two different axial locations: a) at a fixed location X_{fixed} which is invariant for all the *L/D's* investigated and b) at the fan-face $X_{fan\text{-}face}$ which varies with different *L/D's* (since $X_{fan\text{-}face}$ corresponds to the axial location of the leading edge of the fan).

Results at fixed location, X_{fixed}: Fig. 9(a) shows the DC60 value at a fixed location, X_{fixed}, for all the cases of intake-only and the four different fan-intake configurations with different *L/D's*. Recall that the intake-only configuration reported in the figure has been simulated in the absence of the body force model. Also, the flow is considered to be separated when DC60 falls below a critical value (shown by the dashed line in the figure). As evident, the fan has a significant effect on the intake separation. Based on the value of *L/D*, the presence of fan has either a) increased the separation-free angle of incidence ($\Delta\alpha_{sep}$) or b) suppressed the level of the post-separation distortion when compared to the intake-only configuration. When the fan was closest to the lip of the intake (corresponding to *L/D* of 0.17), $\Delta\alpha_{sep}$ was about 5°. This increase of incidence for flow separation decreases as the fan is positioned farther from the lip of the intake. At *L/D* of 0.44, there was no sign of any increase in incidence tolerance ($\Delta\alpha_{sep} = 0$). Secondly, once the flow separates, the fan has the effect of suppressing the level of post-separation distortion. At a given angle of incidence, it was also observed that the closer

the fan, the stronger is the suppression effect. This is also evident from Fig. 9(b) which shows the contours of total pressure for different configurations at the largest incidence condition. Notice in Fig. 9(a) that the DC60 for the intake-fan

L/D=0.44 and intake only cases coincide up to a specific angle of incidence. This is attributed to the fact that the fan is far enough from the plane of interest and would thus have a negligible influence before separation.
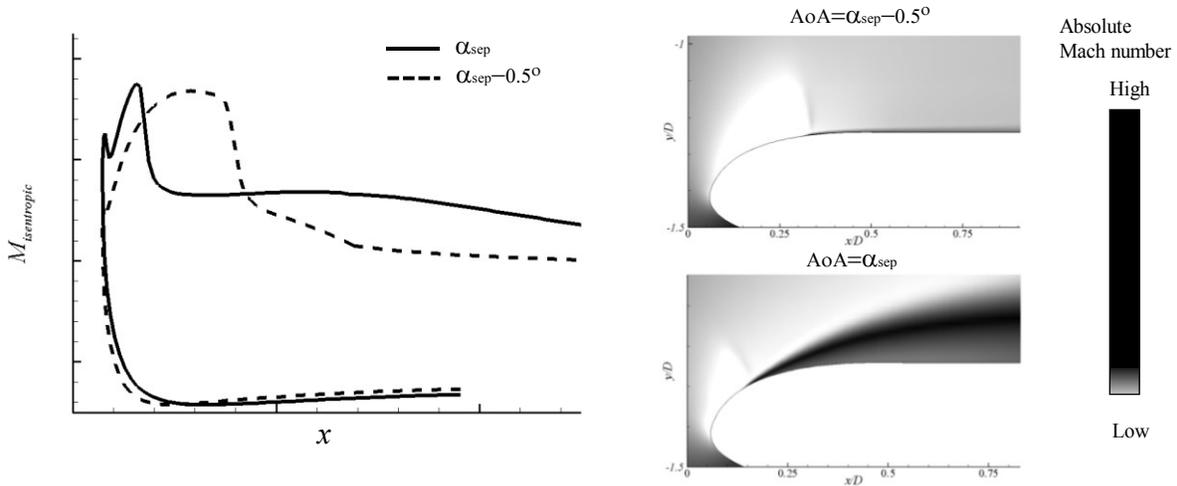

Fig. 8: Isentropic Mach number distribution (left) and according absolute Mach number contour (right) over the model intake-only configuration
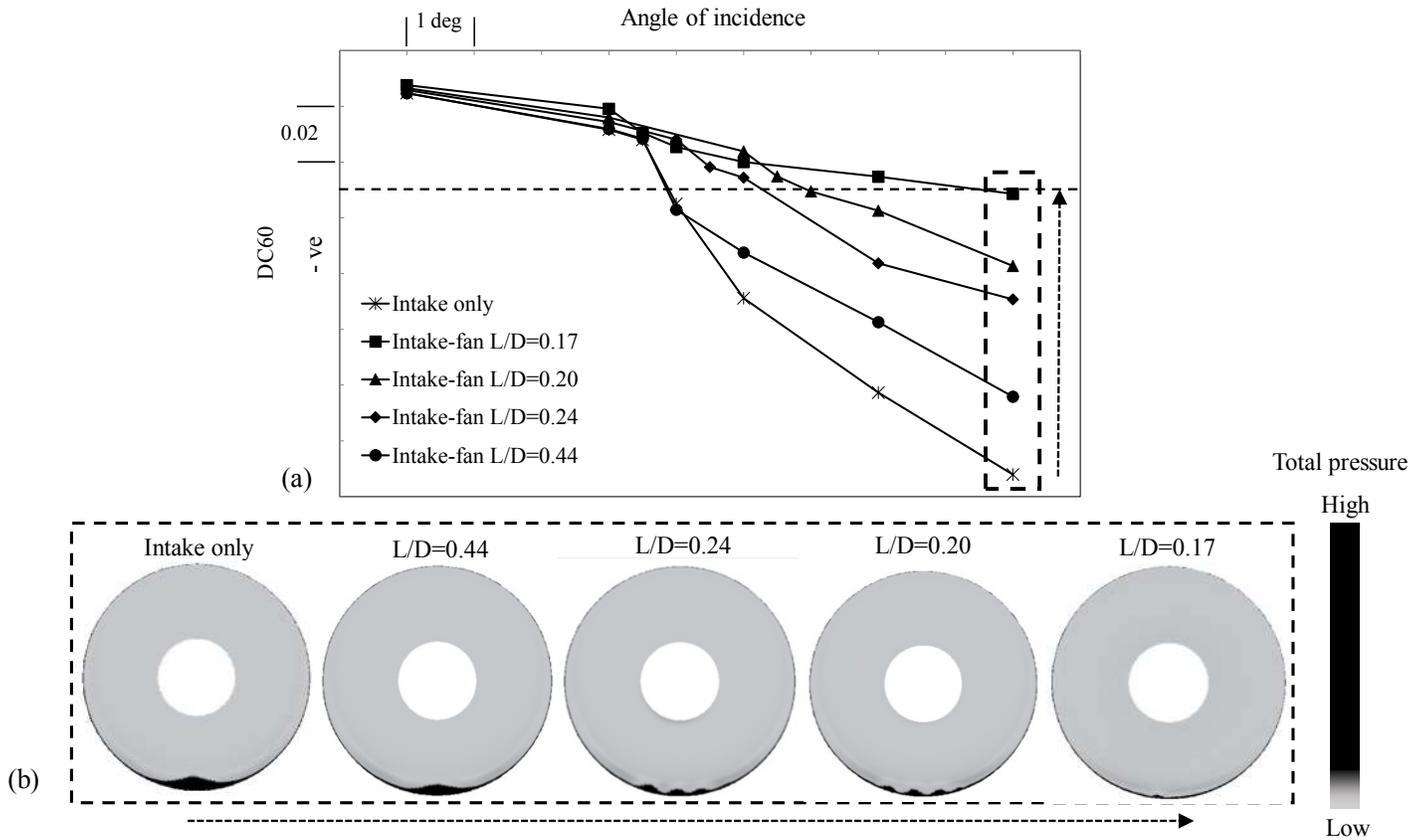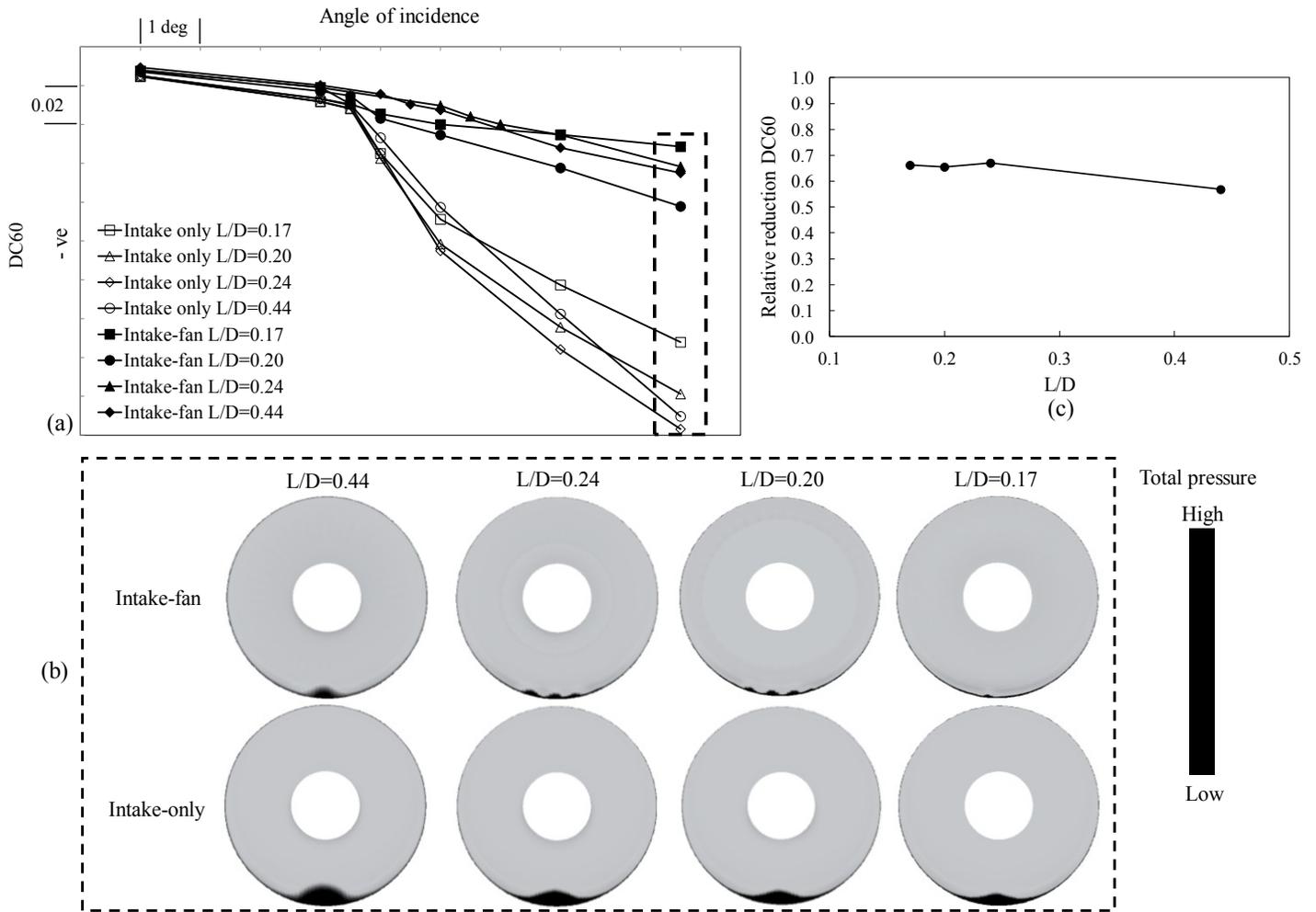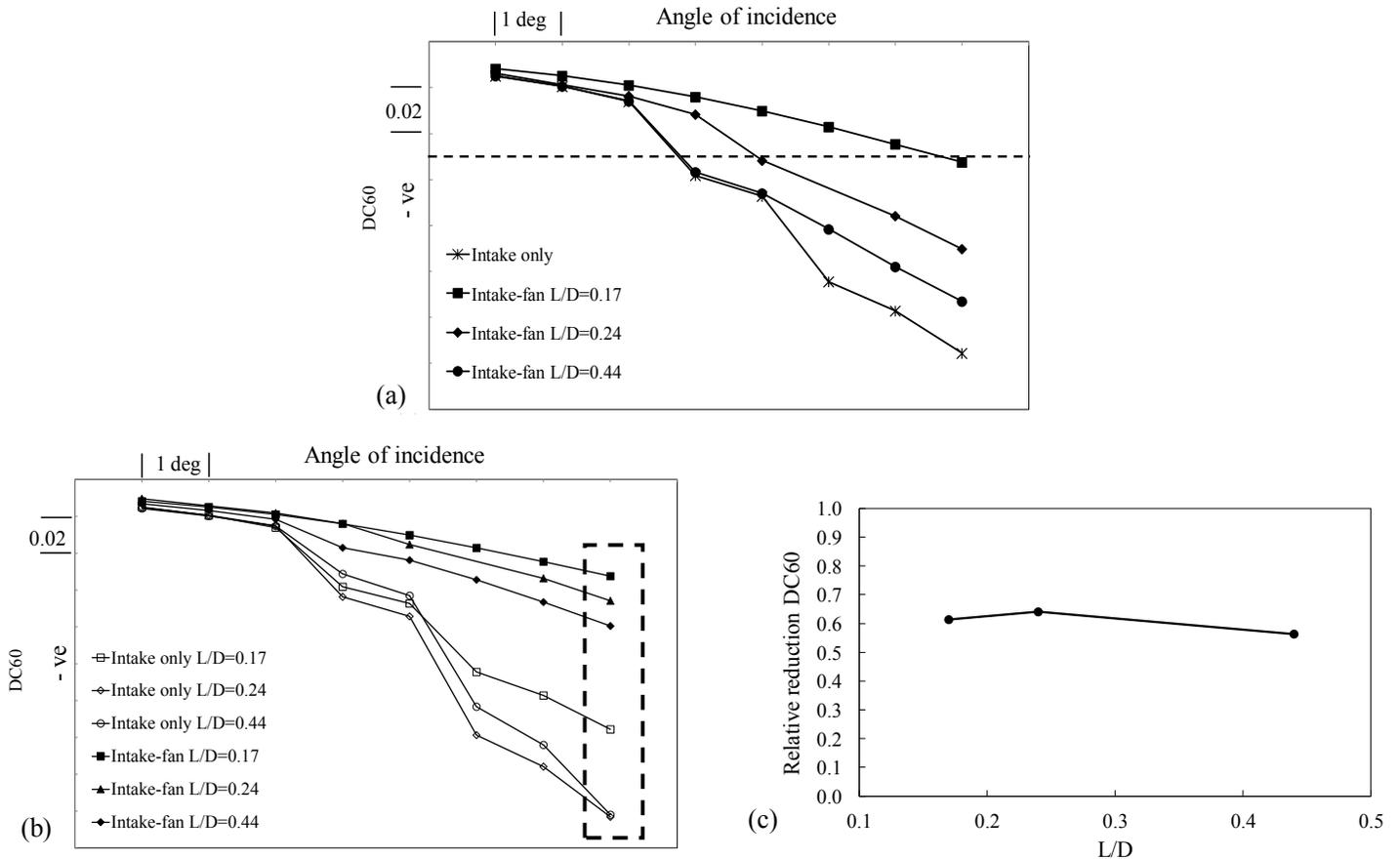

Fig. 9: DC60 values evaluated at the fixed location (a) and total pressure contours under the largest incidence condition (b) for intake-only and intake-fan with different _L/D_ configurations at inlet condition 1

Fig. 10: DC60 values evaluated at the fan-face location (a) and total pressure contours under the largest incidence condition (b) for intake-only and intake-fan with different *L/D* configurations at inlet condition 1 (c) Relative reduction of DC60 at fan-face under largest incidence condition for different *L/D* cases

Results at fan-face location, $X_{fan\text{-}face}$: Fig. 10(a) shows the DC60 value at the fan-face locations, $X_{fan\text{-}face}$. The lines with solid symbols shows the fan-intake configurations and those with hollow symbols represent the intake-only configuration. At the largest incidence condition, Fig. 10(b) compares the contours of the total pressure of both the intake-only and intake-fan configurations at the fan-face, $X_{fan\text{-}face}$. When compared to the intake-only case, it is evident that the fan has suppressed the flow separation at a given angle of incidence. This decrease in the level of distortion appears to be almost constant for all the L/D cases. This observation has been confirmed in Fig. 10(c) where a relative reduction of DC60 between the intake-fan configuration and intake-only configuration has been plotted against L/D. Interestingly, when compared to the intake-only configuration at the same location, the percentage reduction in the separation level due to the fan stays at similar level, all around 60-70%, regardless of the *L/D* value.

Sensitivity to inlet Mach number: To verify the sensitivity of the conclusions drawn so far to the free-stream Mach number, a series of simulations were repeated at a different operating condition (inlet condition 2). When compared to the previous operating condition (inlet condition 1), the free-stream Mach number has been increased by 32%. Fig. 11(a,b) plots the variation of DC60 evaluated at a fixed location, X_{fixed}, and at the fan-face, $X_{fan\text{-}face}$, with angle of incidence. It is evident that the trends are consistent with the low Mach number case (see Figs. 9(a) and 10(a)). Similar conclusions can be drawn even at this operating condition. When compared to the intake-only configuration, the presence of fan a) increased the separation-free angle of incidence ($\Delta\alpha_{sep}$) at lower *L/D's* b) decreased the post-separation distortion level and c) has relatively reduced to DC60 by around 60-70% at the fan-face (see Fig. 11(c)). However, the gain in the incidence tolerance $\Delta\alpha_{sep}$, appears to have decreased by around 1° when compared to the previous operating condition (inlet condition 1).

Fig. 11: DC60 values evaluated at (a) the fixed location and (b) the fan-fan location with different *L/D* configurations at inlet condition 2 (c) Relative reduction of DC60 at fan-face under largest incidence condition for different *L/D* cases

It is worth mentioning that the relative reduction of DC60 at the fan face could be a crucial parameter for the intake design. An intake designer could indeed use this metric to obtain a quick first-order estimate of the fan effect. However, it must be verified if this metric is a constant over a wide range of operating conditions on various speed lines.

Fan-Intake interaction mechanism:
Fig. 12(a) attempts to provide a physical reasoning for the observations made so far. In this plot, the axial variation of the isentropic Mach number distribution over the model-intake for the intake-only and intake-fan configurations were compared. The distributions were extracted at a pre-separated angle of incidence (α_{sep} - 1°). The figure shows that the fan accelerates the flow ahead of the fan-face . The acceleration is primarily due to the redistribution of the mass flow, with the fan-tip drawing more air than the hub. This is evident from Fig. 12(b) which shows the contour plots of isentropic Mach number on the plane located at the fan-face ($X_{fan-face}$) of *L/D*=0.24 for both intake-only and intake-fan configurations. Figure 12(c) also compares the profiles of the radial distribution of normalized mass-flux. The flow acceleration closer to the casing is

responsible for either suppressing the distortion or delaying the flow separation. However, the suction effect decays rapidly upstream of the fan. This explains the observations made in Fig. 9, where the effect of fan on the intake distortion (evaluated at a fixed location) decreased as the fan moved away from the plane of interest. When compared to the intake-only case, the flow is accelerated to a similar level in front of the fan-face for all *L/D* cases. It reinforces the observation made in Fig. 10 and Fig. 11 where the percentage reduction in the distortion level (estimated at the fan-face) due to the fan was almost constant regardless of the *L/D* value.

CONCLUSIONS

In this paper, an extensive numerical study has been carried out on the interaction between the downstream fan and the flow separating over an intake under high incidence. The work provides qualitative insights into the mechanism of fan-intake interaction and it also quantitatively examines the effect of the proximity of the fan on the inlet distortion. The fan proximity is altered using the key design parameter, *L/D,* where *D* is the diameter of the intake and *L* is the distance of the fan from the

intake lip. A number of conclusions can be drawn from this work:

(1) Systematic studies on the model intake-fan configuration showed that the fan is effective in suppressing the intake distortion. This is consistent with the findings in the literature. It also showed that the closer the fan to the intake lip; the stronger the suppression effect is, at a given angle of incidence.

(2) Up to about 5° increase of the separation-free angle of incidence was observed due to the presence of the fan at *L/D*=0.17. This increase of the separation-free incidence decreased with increasing *L/D* (i.e. as the fan moved farther) and there was no sign of delay of separation for the case of *L/D*=0.44.

(3) At the fan-face, there is a considerable suppression effect due to the fan. Interestingly, when compared to the intake-only configuration at the same location, the percentage of reduction of the separation level due to the fan always stays at a similar level, of around 60 to 70%, regardless of the L/D value. The conclusion was also reconfirmed at a higher free-stream Mach number.

(4) Comparison of isentropic Mach number around the
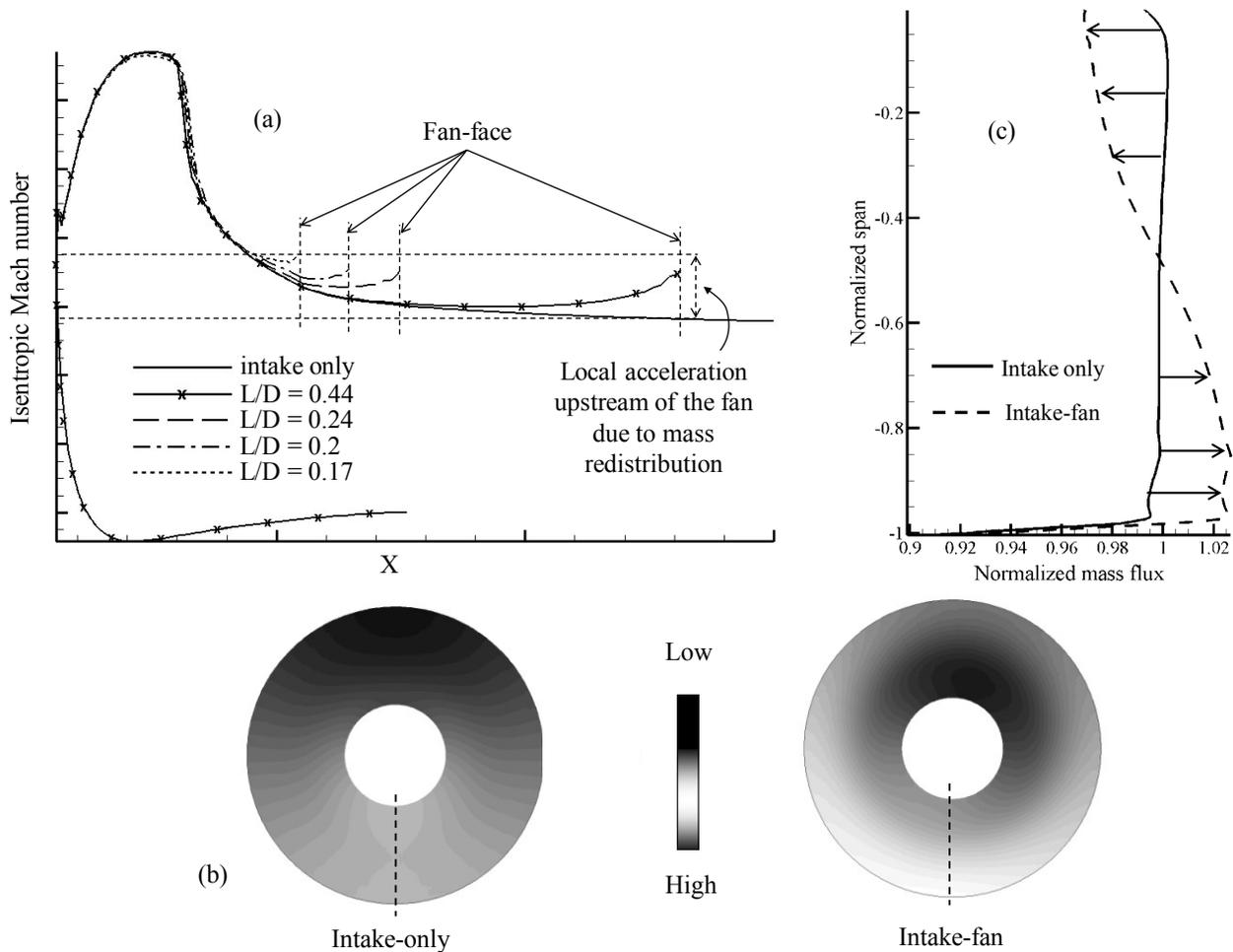
Fig. 12: (a) Isentropic Mach number distributions around the model intake lip for intake-only and intake-fan configurations prior to flow separation ($α_{sep}$ - 1°) (b) Contours of isentropic Mach number on the plane locates at fan-face location (*L/D*=0.24) for both intake-only and intake-fan configuration (c) Radial distribution of the normalized mass-flux extracted at the dashed lines marked in Fig. 12(b)

NOMENCLATURE

D	Diameter
F	Force
M	Million
P	Pressure
V	Velocity
x	X direction of Cartesian coordinate
y	Y direction of Cartesian coordinate
z	Z direction of Cartesian coordinate

Greek Symbols

α	Incidence angle
$\Delta\alpha$	Increase in incidence angle

Subscripts

0	Total value
60	60 degrees sector
sep	Separation
n	Normal direction
p	Parallel
x, r, θ	Cylindrical coordinates, axial, radial and tangential directions

Abbreviations

BFM	Body force model
CFD	Computational Fluid Dynamics
RANS	Reynolds-averaged Navier-Stokes

ACKNOWLEDGMENTS

REFERENCES

[1] Oriji, U. R., and Tucker, P. G., 2014, Modular Turbulence Modelling Applied to an Engine Intake, Journal of TurboMachinery, 136(5), 051004.

[2] Hall, C. A., and Hynes, T. P. (2006), Measurements of Intake Separation Hysteresis in a Model Fan and Nacelle Rig, Journal of Propulsion and Power, 22 (4), 872–879.

[3] Freeman, C. and Rowe, A. L., 1999, Intake Engine Interactions of a modern large Turbofan engine, ASME conference, 99-GT-344.

[4] Larkin, M. J. and Schweiger, P. S., 1992, Ultra High Bypass Nacelle Aerodynamics, Inlet Flow-through High Angle-of-Attack Distortion test, NASA Contractor Report CR-189149.

[5] Boldman, D. R., Iek, C. and Hwang, D. P., 1993, Effect of a Rotating Propeller on the Separation Angle of Attack and Distortion in Ducted Propeller Inlets, NASA Technical Memorandum 105935.

[6] Peters, A., Spakovszky, Z. S., Lord, W. K. and Rose, B., 2015, Ultrashort Nacelles for Low Fan Pressure Ratio Propulsors, Journal of TurboMachinery Vol. 137 / 021001-1.

[7] Hodder, B. K. (1981). An Investigation of Engine Influence on Inlet Performance. NASA CR-166136, 1981.

[8] Kennedy, S., Robinson, T., Spence, S., & Richardson, J. (2014), Computational Investigation of Inlet Distortion at High Angles of Attack, Journal of Aircraft, 51(2), 361-376.

[9] Hsiao, E., Naimi, M., Lewis, J. P., Dalbey, K., Gong, Y., & Tan, C., 2001, Actuator duct model of turboMachinery components for powered-nacelle Navier-Stokes calculations. Journal of Propulsion and Power, 17(4), 919-927.

[10] Iek, C. and Boldman, D., 1993, 3-D Viscous Flow CFD Analysis of the Propeller Effect on an Advanced Ducted Propeller Subsonic Inlet, NASA Technical Memorandum 106240.

[11] Carnevale, M., Wang, F., Green, J. S. and Di Mare, L., 2015, Lip Stall Supression in Powered Intakes, Journal of Propulsion and Power DOI: 10.2514/1.B35811.

[12] Lapworth, B. L., 2004, Hydra-CFD: A Framework for Collaborative CFD development, International Conference on Scientific and Engineering Computation (IC-SEC), Singapore, July 2004.

[13] Watson, R., 2013, Large Eddy Simulation of Cutback Trailing Edges for Film Cooling Turbine Blades, Ph.D. thesis, University of Cambridge, Cambridge, UK.

[14] Sabino L., Tucker, P. G. and Watson, J., Modelling of Coupled Open Rotor Engine Intakes, 48th AIAA Aerospace Sciences Meeting Including the New Horizons Forum and Aerospace Exposition, 4-7 January 2010, Orlando, Florida.

[15] Spalart, P. and Allmaras, S., 1992, A one-equation turbulence model for aerodynamic flows, 30th Aerospace Sciences eeting and Exhibit, AIAA

[16] Cao, T., Hield, P. and Tucker, P. G., 2016, Hierarchical Immersed Boundary Method with Smeared Geometry, AIAA SciTech forum and Exposition, 4 - 8 Jan 2016 in San Diego, California, USA.